

Electrospun Nanocomposite Fibrous Membranes for Sustainable Face Mask Based on Triboelectric Nanogenerator with High Air Filtration Efficiency

Yue Yang ^a, Yuchen Yang ^{a,b}, Jianying Huang ^{a,b}, Shuhui Li ^{c,d,*}, Zheyi Meng ^{e,*},
Weilong Cai ^{a,b,*}, Yuekun Lai ^{a,b,*}

^a College of Chemical Engineering, Fuzhou University, Fuzhou 350116, P. R. China

^b Qingyuan Innovation Laboratory, Quanzhou 362801, P. R. China

^c Department of Chemistry, University College London, London WC1H 0AJ, UK

^d Wenzhou Institute, University of Chinese Academy of Science, Wenzhou, Zhejiang 325000, P. R. China

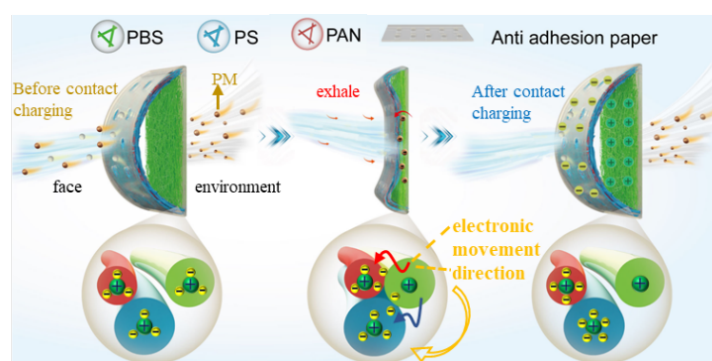
^e State Key Laboratory for Modification of Chemical Fibers and Polymer Materials, Donghua University, Shanghai 201620, P. R. China

Abstract: Air pollution caused by the rapid development of industry has always been a great issue to the environment and human being's health. However, the efficient and persistent filtration to PM_{0.3} remains a great challenge. Herein, a self-powered filter with micro-nano composite structure composed of polybutanediol succinate (PBS) nanofiber membrane and polyacrylonitrile (PAN) nanofiber/polystyrene (PS) microfiber hybrid mats was prepared by electrospinning. The balance between pressure drop and filtration efficiency was achieved through the combination of PAN and PS. In addition, an arched TENG structure was created by using the PAN nanofiber/PS microfiber composite mat and PBS fiber membrane. Driven by respiration, the two fiber membranes with large difference in electronegativity achieved contact friction charging

cycles. The open-circuit voltage of the triboelectric nanogenerator (TENG) can reach to about 8 V, and thus the high filtration efficiency for particles was achieved by the electrostatic capturing. After contact charging, the filtration efficiency of the fiber membrane for PM_{0.3} can reach more than 98% in harsh environments with a PM_{2.5} mass concentration of 23,000 μg/m³, and the pressure drop is about 50 Pa, which doesn't affect people's normal breathing. Meanwhile, the TENG can realize self-powered supply by continuously contacting and separating the fiber membrane driven by respiration, which can ensure the long-term stability of filtration efficiency. The filter mask can maintain a high filtration efficiency (99.4%) of PM_{0.3} for 48 consecutive hours in daily environments.

Keywords: Electrospinning; Self-powered filter structure; Triboelectric nanogenerator; Air filtration

TOC figure:



*Corresponding author. E-mail address: shuhui.li@ucl.ac.uk (Shuhui Li); mengzheyi@dhu.edu.cn (Zheyi Meng); wl.cai@fzu.edu.cn (Weilong Cai); yklai@fzu.edu.cn (Yuekun Lai).

1. Introduction

Due to the outbreak of coronavirus in 2019 and the acceleration of urbanization and industrialization in developing countries, the increased air pollution seriously endangers public safety and human health, and has become a highly concerned issue in society [1-6]. As one of the main culprits of air pollution, the suspended particulate matter (PM) with different sizes in the atmosphere has a serious impact on air quality and visibility. Particularly, the microparticles with high permeability (aerodynamic diameter $\leq 0.3 \mu\text{m}$) suspended in the atmosphere can carry a large number of toxic and harmful substances and fatal viruses, and penetrate into the human bronchi and alveoli through the human respiratory, which will be harmful to the human body after long-term exposure to PM [2, 7-15]. The protective face masks are the most effective route to product to prevent the spread of viruses and protect human health. Notably, N95 mask is assigned to a filtration efficiency reached to or over 95 % on $0.3 \mu\text{m}$ sized sodium chloride aerosols (average diameter of aerodynamic mass) and effective filtration time of 8 h at a flow rate of 85 L/min, which has been professionally confirmed to be adequate for daily protection [16-17]. Structurally, PP (polypropylene) fiber melt blown for N95 masks has the characteristic of high layer thickness, providing sufficient physical barriers, but the high layer thickness can lead to an increase in pressure drop. To further coordinate the filtration efficiency and breathing resistance, the PP fibers are charged via corona discharge method to enhance capture of N95 filters to $\text{PM}_{0.3}$ via electrostatic interaction [18-22]. However, the charge dissipation of filters in humidity environment will undoubtedly lead to the dramatic decrease of filtration efficiency. In

summary, the N95 filtering facepiece respirators would be limited for reusing considering hygiene, damage, increased breathing resistance and the decreased filtration efficiencies [19, 23-24]. Therefore, it is urgent to develop a filter material with excellent filtration efficiency for particles and long-term stable charge.

Triboelectric nanogenerators (TENG) can effectively collect various forms of low-frequency mechanical energy through contact electrification and electrostatic induction and convert it into electrical energy, showing significant superiority and prospects for effectively capturing PMs by long-range electrostatic interaction [25-28]. For instance, Bai et al. designed washable TENG-based air filter which consists of multilayer polytetrafluoroethylene (PTFE) and nylon microfiber fabrics and can be utilized as the reusable face mask [9]. Santra et al. developed TENG-based face mask for removing PMs by combining nylon, cotton and polyacrylonitrile microfibers [23]. Besides, in contrast to traditional microfibers or ultrafine fibers, nanofiber mats produced by the electrospinning technique exhibit superior filtration efficiency due to the fine fiber size, small pores and high porosity [29-33]. Thus, developing electrospun nanofiber-based TENG may help to obtain the high-performance filters by synergistic effect of mechanical interception via nanofibers and electrostatic attraction via triboelectric charges. Gu et al. connected electrospun polyimide (PI) nanofiber membranes to a rotating triboelectric nanogenerator (R-TENG) [34]. Thereby charging the PI fiber membrane to improve the filtration efficiency of the PI fiber membrane. Especially for PM particles with a diameter of less than 100 nm, the removal efficiency increased from 27.1% to 83.6%. Similarly, by connecting a triboelectric nanogenerator also can add

electric charge to the PP melt blown cloth and improve the life span of the mask [35]. Despite of above advances in TENG-based air filters, the required external power supply for continuously generating electrostatic charges critically limits their practical applications. Fortunately, the self-charging nanofiber face masks can constantly generate electrostatic charges by contact friction of different fibers driven by respiration without external power sources, which may enable filters of stable and long-term filtration performance and thus attracts extensive interest among researchers. Cho et al. mixed hexadecyltrimethylammonium bromide (CTAB) and montmorillonite (MMT) clay in N, N-Dimethylformamide (DMF) using a polybutylene terephthalate (PBAT) matrix. Through electrospinning, CTAB-MMT is coated with PBAT, thereby improving the triboelectric effect and making the electrospun fiber membrane has high filtration efficiency (98.3%, $PM_{0.3}$) [36]. Fu et al. obtained cellulose hydrogel cross-linking and regeneration, and then in situ synthesized conductive metal organic framework (Ni HITP) on cellulose aerogel to prepare cellulose aerogel/Ni HITP (CA/Ni hexaminotriphenylene (HITP)) composite. A self-powered filter material composed of CA/Ni HITP and PVDF electrospun fiber membrane can achieve a filtration efficiency of 95% for $PM_{0.3}$ [37]. Liu et al. connected polyvinylidene fluoride electrospun nanofiber film (PVDF-ESNF) with copper film using rubber, and designed a mask containing an air outlet and an air inlet to achieve contact friction charging between PVDF-ESNF and copper film through breathing, improving the filtration efficiency of the fiber material (99.2%, $PM_{1.0}$) [8]. Nevertheless, the related research is still at initial stage. In order to achieve frictional electricity generation of respiratory driving

materials, the existed self-powered TENG air filters driven by respiration generally had complex structure and complicated preparation process. Therefore, it is necessary to simplify the structure and preparation process of TENG filter materials.

In this work, a novel self-powered air filter mask with simple structure was designed by utilizing fiber membrane adhesion and separation driven by respiration. The air filter mask composed of two different fiber membranes was made by the facile electrospinning technology. Firstly, the PAN nanofiber /PS microfiber was prepared through the co-electrospinning process, while the coarse PS microfibers were used as the supporting frame to improve the permeability, and the fine PAN nanofibers provided good filtration efficiency. Secondly, the PBS electrospun nanofiber membrane with the lower electronegativity was prepared. Then two anti-adhesion papers with breather holes were pasted on the back of the two fiber membranes to form an arched self-powered supply structure, as shown in Fig. 1a. The air flow generated by breathing promotes the circular contact and separation of fiber membranes, which induces that electrons move directionally from the PBS fiber with low electronegativity to the PAN nanofiber/PS microfiber composite mat with high electronegativity. Due to the synergistic effect of electrostatic capture and physical interception and the composite structure, the prepared fibrous filter exhibits excellent filtration performance. Under severe air conditions (The concentration of $PM_{2.5}$ ($\rho_{PM_{2.5}}$) is $23,000 \mu\text{g}/\text{m}^3$), the filtration efficiency of $PM_{0.3}$ is still above 98.5%, and the pressure drop is only 53 Pa. As shown in Fig. 1b, compared to some recent distinguished works such as the perfluorinated electret nanofibers [13], triboelectric core-shell nanofibers [36],

modified electrospinning nanofiber/nanonet [38, 39], metal organic framework modified aerogel [40], PP melt blown fabric (N95 mask middle layer), at the same flow rate (32 L/min), our designed filter shows the superior filtration performance (99.98% of high PM_{0.3} filtration efficiency and 35 Pa of low pressure drop) measured by the filter material comprehensive performance test bench (LZC-K₁, Fig. S1b). In addition, it can generate electric charge all the time during the respiration process, which endows itself with long-term and stable filtration efficiency. The self-powered device also can continuously generate an open circuit voltage of about 8 V during the contact and separation cycle (Fig. 1c).

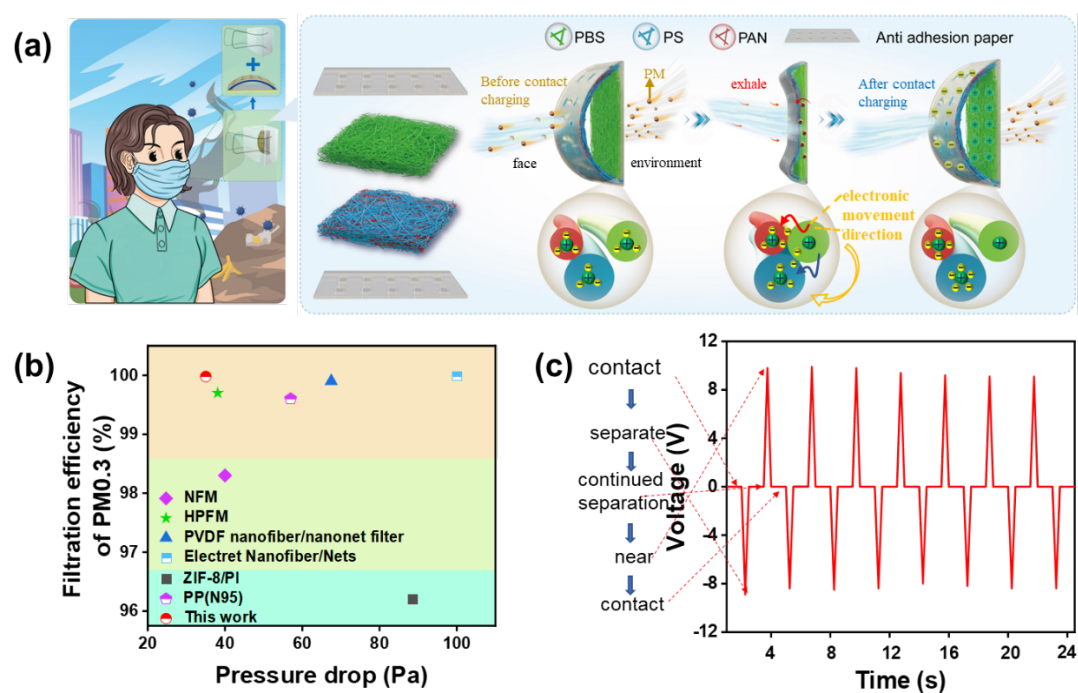


Fig. 1 (a) Schematic diagram of self-powered filter mask(left) and self-powered principle (top right), (b) Performance comparison between the self-powered filter mask designed in this research and other similar work, and (c) Measurement of open circuit voltage of self-powered structure in contact separation process using AC ammeter.

2. Experimental Part

2.1 Materials & Reagents

Polybutylene succinate (PBS, Mw: 200,000), Polyacrylonitrile (PAN, Mw: 85,000), Chloroform, Isopropanol (99.7%) and N-N dimethylformamide (DMF, 99.5%) were purchased from Shanghai Macklin Biochemical Technology Co., Ltd. Polystyrene (PS, general type III, extrusion and food use, Mw: 104.14) was provided by from Shanghai Aladdin Bio-Chem Technology Co., Ltd.

2.2 Preparation of Nanofiber Membrane

(1) Preparation of PBS nanofiber membrane

Firstly, prepare a 12wt% PBS spinning solution. Add a certain amount of PBS particles to a mixed solution of chloroform and isopropanol (chloroform: isopropanol=7:3), where chloroform is used as a solvent and isopropanol is used as a stabilizer [41]. To prepare PBS nanofiber membrane, the as-prepared PBS spinning solution was added into the syringe, an anti-adhesion paper was used as the receiving substrate. The experimental parameters were set as follows: the propulsion rate was 2 mL/h, the spinning voltage was 15 kV, the receiving distance from syringe to receiving substrate was set to 15 cm, the PBS nanofiber membrane was obtained after spinning for 4 h with a spinning temperature of 25 ± 5 °C and 60% of humidity [42].

(2) Preparation of PAN nanofiber/PS microfiber composite mat

12 wt% of PAN and 24 wt% of PS spinning solutions were firstly prepared in DMF solvent, respectively [43, 44]. Then, the PAN and PS spinning solutions were separately injected into two syringes. Subsequently, the two syringes were assembled on an electrospinning machine and kept the same propulsion rate of 1 mL/h. Apart of the

spinning voltage is 20 kV, the other parameters are the same as that of PBS nanofiber membrane. After spinning for 4 h, the PAN nanofiber/PS microfiber composite mat was obtained [45].

2.3 Structural Characterization

The surface morphology and structure of fibrous mats were observed by FE-SEM (S-4800, Hitachi). The wettability of fiber membrane was characterized by water contact angle meter (OCA 20), and the open circuit voltage of self-powered filter was measured by a multimeter (VC890E) and digital source meter respectively (Keithley 2450). The surface potential of the fiber membrane was tested by an electrostatic field meter (FMX-003). Number of particles was tested using a particle counter (DT-9883M). Mechanical tests were performed using a multifunctional fabric tester (KONGDA, HD026S-100).

2.4 Performance Test

(1) Test of filtration efficiency

The filtration efficiency was determined by the number of particles upstream and downstream of the filtration device (recorded as N_1 and N_2 , which was detected by the particle counter), and the efficiency can be calculated by $\eta = (N_1 - N_2) / N_1 \times 100\%$. Number of particles before and after filtration was tested using a particle counter (DT-9883M, PM size range: 0.3-10 μm) [37,46]. The pressure drop was characterized by the pressure drop measuring instrument (Testo 510).

(2) Measurement of surface potential and calculation of electric field strength of single fiber

The surface potential of the fiber membrane can be measured by the surface potential meter. The surface potential measuring instrument was put 2 cm above the fiber membrane, and the average value after 5 times of testing was recorded as the surface potential of the fiber membrane. In addition, the electric field strength of a single nanofiber was measured according to the following equation (1), the action range of electric field force can also be obtained by observing the distribution of electric field force. The calculation formula is as follows [47]:

$$E = \frac{U}{\pi\varphi(1-p)(\sqrt{R^2+H^2}-R)L} \quad (1)$$

Where, U (V) is the surface potential, φ (m) is the fiber membrane thickness, L (m) is the distance to a single fiber, and P is the porosity ($P=\omega/\rho$, ω is the mass ratio, ρ is the density), R (m) is the radius of the induced light spot when testing the surface potential, and H (m) is the distance between the surface potential meter and the sample.

3. Results and Discussion

3.1 Morphology and Hydrophobicity of PAN/PS composite mat

The PAN, PS and PBS have a significant difference in electronegativity, which can realize the directional movement of electrons through the contact of polymer fibers. However, the prepared PAN nanofibers presented the small pore diameter (Fig. 2a) due to their relatively thin fiber diameter of 0.2-0.4 μm (Fig. 2d), which leads to both high filtration efficiency and high pressure drop of the filter. Conversely, the obtained PS fibers with the thicker diameter of 3-4 μm (Fig. 2b and 2e) possess superior air permeability but low filtration efficiency. In comparison to PAN, PS possesses lower

dielectric constant and charge density, which resulted in the insufficient stretching of electrospun PS jets and thus the curly and fluffy structure of PS microfiber mat. Thus, the composite fluffy structure consisting of the thicker PS microfibers and the thinner PAN nanofibers can simultaneously endow the filter with excellent filtration efficiency and improved air permeability. Specifically, the PS microfibers and PAN nanofibers were mixed with different volume ratios to form the various composite membranes by the co-electrospinning technique (Fig. S1), and the preparation parameters can be found in Table S1. As expected, the prepared PAN/PS fiber mats with different base weights exhibit the $PM_{0.3}$ filtration efficiency of over 95% and the filtration resistance of below 145 Pa even at a flow rate of 85 L/min. PAN/PS fiber mat with the base weight of 5 g/m^2 shows the best quality factors (Fig. S1d) but is vulnerable due to its thin thickness. Considering the mechanical performance requirements of friction charging, thus, the composite PAN/PS fiber membrane with the basis weight of 10 g/m^2 is selected for subsequent experiments. The optimized composite membrane has filtration efficiencies of 99.98% and 97.53% for $PM_{0.3}$ at a flow rate of 32 L/min and 85 L/min, respectively, with a pressure drop of only 35 Pa and 85 Pa. Compared to common PP melt blown fabrics, it has better performance. The morphology of obtained blended fiber membrane is presented in the Fig. 2c. In the mapping image, the N elements are uniformly distributed, which strongly proves that the PAN nanofibers are well blended with the PS microfibers (Fig. 2f).

In order to obtain the optimal filtration efficiency of the blended PAN nanofiber/PS microfiber composite mat, the composite mats with various volume ratios of 2:1, 1:1

and 1:2 were prepared, which were labeled as PAN/PS2-1, PAN/PS1-1 and PAN/PS1-2, and their thickness measured by a digital micrometer gauge (25 × 30 cm, flat head) are 0.18 mm, 0.27 mm, and 0.50 mm, respectively. From Fig. 2g-i, the increased coarse PS microfibers within composite mats can separate the fine fibers to decrease the packing density of fine PAN nanofibers and thus improve air permeability. The hydrophobicity of the PAN/PS composite mat ensures that the filter can effectively prevent the moisture generated by breathing from entering the fiber membrane during the wearing process of the human body, thus avoiding the rapid dissipation of electric charges. The water contact angles of various PAN/PS composite mats were measured. All blended fiber membranes exhibited high hydrophobicity. With the increased ratio of PS microfibers to PAN nanofibers, the composite mats also showed the improved hydrophobicity and the contact angle of the PAN/PS1-2 reached to 148.4°, which results from that increased PS microfibers with hydrophobic benzene rings can effectively enhanced hydrophobicity of composite mat. Moreover, as shown in Fig. S2, the hydrophobic property of the PAN/PS (142.9 ± 0.5°) composite mat is higher than that of the PP melt blown nonwoven (135.1 ± 0.4°) used as the intermediate layer of the mask. Obviously, the PAN/PS composite mat has better hydrophobicity than ordinary filter materials, and can more effectively prevent water vapor from infiltrating and thereby affecting filtration efficiency.

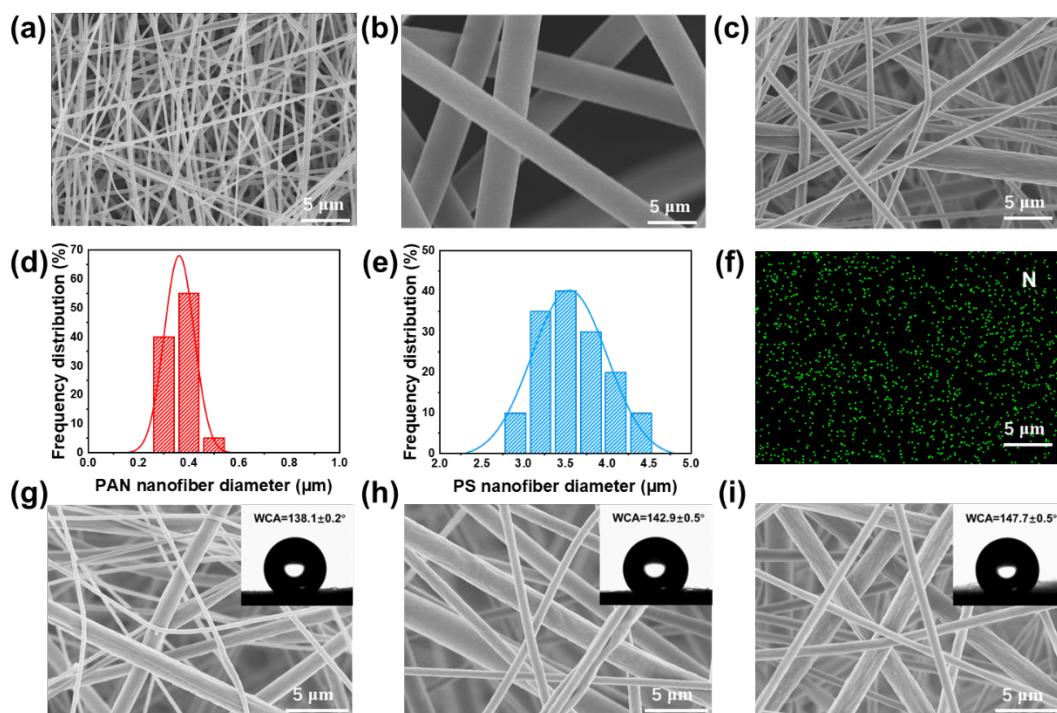


Fig. 2 (a) SEM image of PAN fiber, (b) SEM image of PS fiber, (c) SEM image of PAN/PS fiber, (d) diameter distribution of PAN fiber, (e) diameter distribution of PS fiber, (f) distribution diagram of N element in PAN/PS fiber mats, SEM images and water contact angle of composite membrane when PAN: PS is (g) 2:1, (h) 1:1, and (i) 1:2.

3.2 Effect of Different Injection Ratio on Filtration Performance and Surface Potential of PAN/PS composite mat

The filtration efficiencies of the as-prepared PAN, PS, PAN/PS composite mat were investigated. A 5 cm × 5 cm piece was cut and mounted in the self-built filtration device (Fig. 3a), the cross-sectional area of the air pipe is 7 cm², the burning incense was used to generate oily PMs, a vacuum pump with a 0.18 m/s of air velocity was applied to push the particles passing through the filters. The filtration efficiency and the

pressure drop of the fiber membrane are shown in Fig. 3b. the PAN nanofiber membrane shows the 99.7% PM_{0.3} removal but also high pressure drop of 428 Pa, which cannot meet the requirements of human respiration. The PS microfiber membrane has a low pressure drop of 28 Pa, but its filtration efficiency is only 54%. However, the PAN/PS composite mat showed excellent PM_{0.3} filtration efficiency of 93.2% and the pressure drop of only 48 Pa. The quality factors (QF) of three kinds of fiber membranes are calculated by equation (2):

$$QF = \frac{-\ln(1-\eta)}{\Delta P} \quad (2)$$

Among them, η is the filtration efficiency, ΔP is the pressure drop [48].

It can be seen that the QF value of PAN/PS composite mat was much higher than that of PAN and PS fiber membrane. As shown in Fig. 3e, the QF value of both PAN mats and PS mats is below 0.03, far lower than that of PAN/PS composite mat. It indicates that the blending of PAN nanofibers and PS microfibers can achieve a better unity of filtration performance and permeability of fiber membrane.

To further determine the filtration efficiency of the PAN/PS fiber mats with various blending ratios, the PAN/PS2-1, PAN/PS1-1 and PAN/PS1-2 were prepared for further measurement. The filtration efficiency and pressure drop of the PAN/PS composite mat were shown in Fig. 3c). The PAN/PS2-1 composite mat shows the highest PM_{0.3} filtration efficiency (>99%) and its filtration efficiency does not show significant decrease after 60 min of filtration. However, with the increase of PS microfiber ratio, the fiber membrane gradually becomes fluffy and presents the decreased filtration efficiency. The PM_{0.3} filtration efficiency of the PAN/PS1-1 composite mat decreases

to 94%, but it remains above 90% after 60 min of filtration. But the $PM_{0.3}$ filtration efficiency of the PAN/PS1-2 composite mat decreases to below 90%, and shows an obvious decrease after long-term filtration. However, the pressure drop of the three fiber membranes after filtration is another vital parameter to consider. This is because the fine PAN nanofibers have a good physical interception effect on particles. The higher the content of PAN nanofibers, the better the filtration efficiency. Although the filtration efficiency of PAN/PS2-1 fiber membrane is the best, the pressure drop reaches to 120 Pa, which is far beyond the requirements for masks. With the increase of PS content, the pressure drop gradually decreases. The pressure drops of PAN/PS1-1 and PAN/PS1-2 are 48 Pa and 43 Pa respectively. This is because inside the PAN/PS co spun fiber membrane, the bulky PS fiber supports the whole frame, providing good air permeability, and the internal entangled PAN fiber provides good filtration efficiency. When the ratio of PAN and PS is 1:1, the balance between filtration efficiency and permeability is well achieved. The calculated quality factor is shown in Fig. 3f. It can be seen that the quality factor of PAN/PS1-1 is relatively higher, reaching 0.056. At the same time, the pressure drop of PAN/PS1-1 is only 43 Pa, which is suitable to be used as a face mask for human body.

The water vapor generated by breathing will cause the mask to become wet after wearing for a long time, which will lead to the reduction of filtration efficiency. Therefore, it is necessary to explore the filtration performance of the filter under high humidity. Adjust the humidity of fume hood to 70%, 75%, 80% and 85% through humidifier to measure the filtration efficiency of PAN/PS1-1 fiber membrane under

different humidity (Fig. 3d). With the increase of the humidity, the filtration efficiency of the fiber membrane gradually decreases. However, even under the high humidity of 85%, the fiber membrane still has a $PM_{0.3}$ filtration efficiency of 80% and the QF value of 0.035 (Fig. 3g). This may result from the fact that the hydrophobicity of the fiber membrane effectively prevents the infiltration of moisture, which does not greatly affect the filtration performance of the fiber membrane. And the pressure drop of mat slightly increases with the increase of humidity, which can be attributed to the fact that a small amount of water vapor adheres to the surface and interior of the fiber and seals the internal pores with the increase of humidity. In addition, the wet fiber membrane may result in the collapse of original fluffy structure, which will also increase the pressure drop of the filter [49]. However, due to the hydrophobicity of the fiber membrane, only a small portion of water vapor permeates into the fibers, resulting in an increased pressure drop only about 5 Pa. The above results indicate that the PAN/PS composite mat exhibits superior filtration performance even at high humidity.

The surface potential of PAN/PS composite mat with different proportions and PBS membrane were measured with a surface potential meter, and calculate the electric field strength of a single fiber was calculated according to Formula (1) (Fig. 3h-j). It can be seen that the electric field strength of a single fiber in the blend fiber membrane increases first and then decreases with the increases of the PS proportion. This is because the electron transfer capabilities of PAN and PS are different, so there is a potential barrier at the interface between PAN and PS, resulting in the accumulation of charges at the interface. This phenomenon is called the Maxwell Wagner effect, and it

is also the essential reason for the improvement of fiber electret performance under the coupling effect of PAN and PS. When the PS content is too high, the potential barrier caused by different electron transmission capabilities decreases, the interface area of charge accumulation decreases, leading to the reduction of the electric field strength of a single fiber. When the ratio of PAN: PS is 1:1, the surface potential increases significantly to 3.5 kV, which is the optimal one among all of the samples. And the action range of electric field force reaches about 3.5 cm. Such an action range of electric field force can completely capture the particulate matter around and inside the filter membrane.

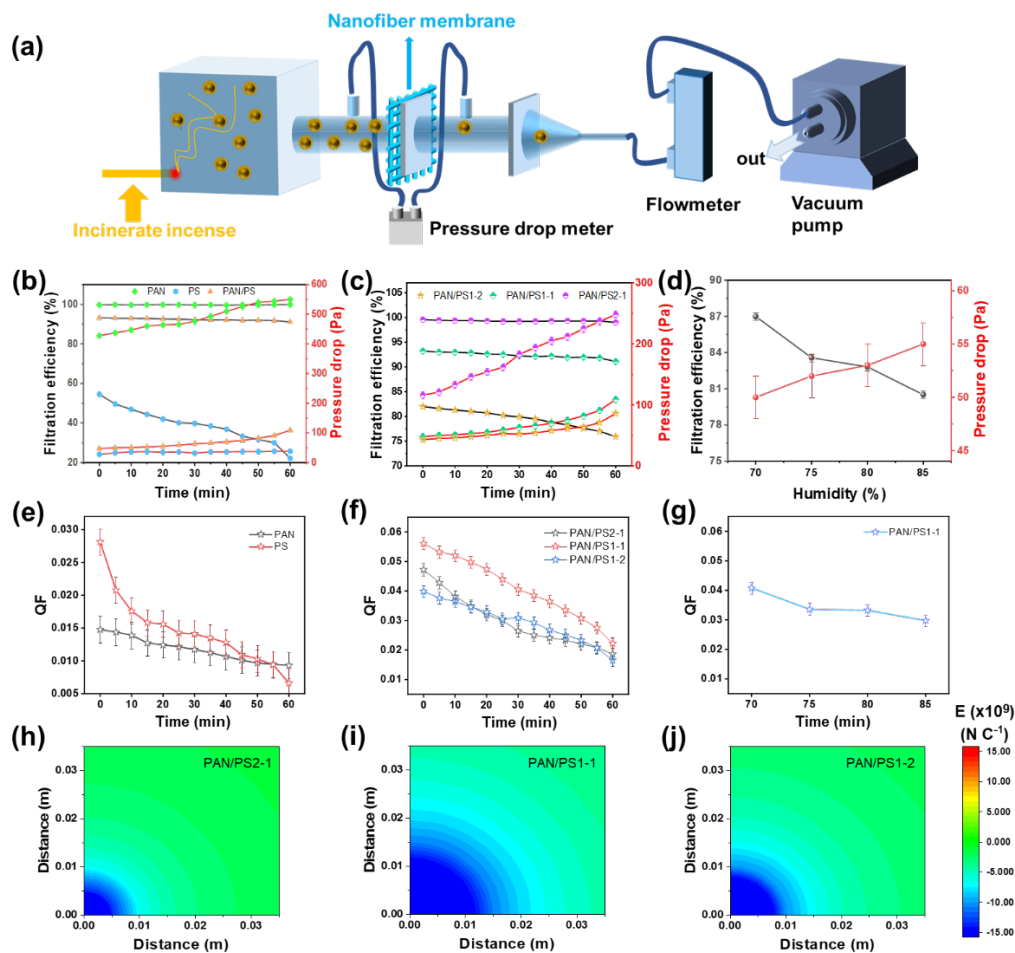


Fig. 3 (a) Schematic diagram of filtration device, (b) filtration efficiency and pressure

drop of PAN, PS, PAN/PS fiber membranes, (c) filtration efficiency and pressure drop of PAN/PS2-1, PAN/PS1-1, PAN/PS1-2 fiber membranes, (d) filtration efficiency and pressure drop of PAN/PS1-1 at different humidity, (e) quality factor of PAN, PS fiber membranes, (f) quality factor of PAN/PS2-1, PAN/PS1-1, PAN/PS1-2 fiber membranes, (g) quality factor of PAN/PS1-1 at different humidity, (h) PAN/PS2-1, (i) PAN/PS1-1, (j) PAN/PS1-2 fiber membrane Electric field strength of single fiber.

3.3 Construction of TENG and Charging Performance

PBS fiber membrane with lower electronic acquisition capability than PAN/PS composite mat was also prepared by electrospinning method. Ability of different materials to gain or lose electrons are summarized in Fig. S3. SEM images of PBS fiber mats prepared under different voltages are shown in Fig. S4. The PBS fiber membrane prepared at a voltage of 10 kV has the poor fiber morphology such as uneven fiber diameter and a large number of beads. As the voltage rises to 12 kV, the fiber evenness has been improved, and the number of beads has also decreased. When the voltage reaches to 15 kV, the beads disappear and the fibers are evenly distributed. The obtained PBS fiber mat is assembled with PAN/PS fiber composite mat, thus forming into friction nano generator (TENG), as shown in Fig. 4a. The spinning parameters and basis weight of PBS fiber membrane were optimized (Fig. S5). Al sheets were attached on the back of the two fiber membranes, respectively, and then connect them with the digital source meter. When an external mechanical force is applied to the prepared TENG, the PBS fiber membrane will contact with the PAN/PS composite mat. Depending on the ability of gaining and losing electrons, the surfaces of the two kinds

of mats will have equal amount of positive and negative charges of opposite polarity. When the applied external force disappears or the applied mechanical force separates the two mats, there will generate an electric potential difference between two electrodes, allowing the electronic migration between the two electrodes before they are far enough apart. Once the external mechanical force is applied again, the distance of the two friction materials decreases, and the difference of electric potential will drive the electrons to flow in the opposite direction again, generating the current in the opposite direction. Fig. 4b shows the open circuit voltage of the PAN/PS-PBS composite membrane measured by the digital source meter. With the continuous contact and separation between the PAN/PS composite mat and the PBS fiber mat, the alternating open circuit voltage in the opposite direction is generated, which can reach to more than 8 V at most, indicating that the filter has good self-powered supply performance.

Fig. 4c shows the schematic diagram of measuring surface potential with FMX-003 surface potential measuring instrument. The surface potential measuring instrument was put 2 cm above the fiber membrane, and the surface potential in a certain of irradiation area was obtained by the probe at the bottom of the measuring instrument. The electric field strength of a single fiber can be calculated by Formula (1). An arched self-power supply structure was created by attaching anti-adhesion paper on the back of the PAN/PS composite mat and the PBS fiber membrane (Fig. 4d). When air flow was applied, the two fiber membranes fully contacted. Once the air flow was removed, the PAN/PS fiber composite mat bounded back to original place and the two fiber membranes separated immediately, thus completing the primary charging. Using

the surface potential meter to measure the surface potential of the fiber membrane after contact and separation as well as the change of the surface potential during continuous contact and separation (Fig. 4e and f). When the PAN/PS composite mat contacts and separates from the PBS fiber membrane, the surfaces of the two fiber membranes were charged with opposite charge, respectively. The surface potential of the PAN/PS composite mat was -3.5 ± 0.2 kV, and the surface potential of the PBS membrane was 2 ± 0.2 kV, which is consistent with the friction charging mechanism. The surface potential of the two fiber membranes after 10 cycles of contact-separation were measured (Fig. 4f). Before starting contact charging, the two fiber membranes are treated with ethanol to eliminate the surface potential of both the PAN/PS composite mat and the PBS fiber membrane closer to 0 (0.04 kV, -0.03 kV). With the increase of contact-separation times, the surface potential of the two membrane surfaces gradually increases, and then reaches equilibrium after six or more consecutive cycles. The charge dissipation rates on fiber membranes of various polymers are different within the same time, and the surface potential is inconsistent due to the different degree of charge dissipation at the time of detection. To confirm this conjecture, the same charging operation was performed using different substrate materials (PVC), as shown in Fig. S6, the results show that both PBS fiber membrane and PAN/PS composite mat exhibits negative potential, while the PVC film as the substrate exhibits positive potential. This is because the electronegativity of PVC is smaller than that of PBS, PAN, and PS. During the contact process, electrons move from the PBS fiber membrane and PAN/PS composite mat to the PVC film, rather than between the two fiber membranes, resulting

in the negative charge on the PAN/PS and PBS fibers and the positive charge on the PVC film. It is worth noting that even though the charge characteristics of the PAN/PS composite mat measured using surface potential are consistent with those of the PBS fiber membrane, there are still differences in numerical values. However, as a substrate, the surface potential of PVC films measured by a surface potential measuring instrument, regardless of whether they are in contact with PAN/PS or PBS, is basically equal, which is consistent with the assumption that "the difference in surface potential measurement values is related to the different dissipation rates of charges in different materials". Fig. 4g shows the electric field strength of a single fiber of two fiber membranes after contact charging. As the surface potential of PAN/PS composite mat was opposite to that of PBS fiber membrane, the direction of electric field strength of single fiber is also opposite. In addition, the electric field force range of a single PBS fiber is only 0.9 cm, which is much smaller than that of PAN/PS composite mat (3.5 cm), which is related to the surface potential of the fiber membrane.

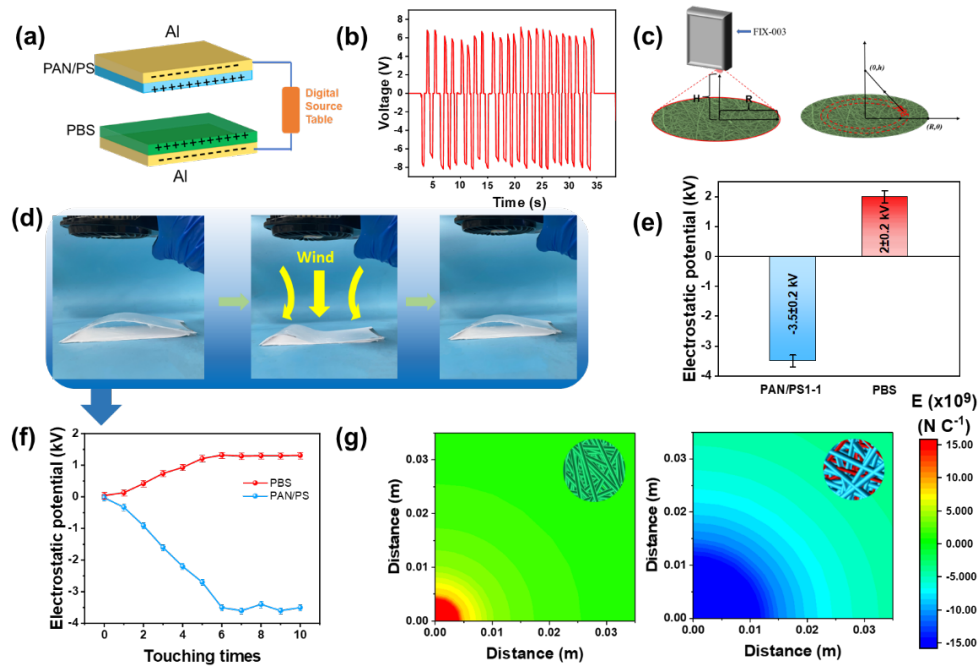


Fig. 4 (a) Schematic diagram of the PAN/PS-PBS (TENG) structure, (b) Measurement of open circuit voltage of self-powered structure with digital source meter, (c) Schematic diagram of surface potential measurement, (d) Contact-separation of self-powered structure when air flow passes through, (e) Surface potential of the PAN/PS composite mat and PBS fiber membrane after contact separation cycles, (f) Change of surface potential of the PAN/PS composite mat and PBS membrane during cyclic contact-separation, (g) Electric field strength of PBS and PAN/PS single fiber after contact-separation.

3.4 Filtering Performance and Charging Performance of Self-Powered Respirator

Fig. 5a shows the optical picture of the air filtration mask with TENG structure. The arched self-charging structure composed of PAN/PS composite mat and PBS fiber membrane based on anti-adhesion paper can be put into the wearable frame to assemble an air filtration mask. The wind energy generated by breathing will cause the upper arch

structure contact with the lower part, which contributes to generate friction charges and improve the filtration efficiency of the nanofiber membrane. Through the SEM analysis of the filtered fiber membrane (Fig. 5b), the oily particles were mostly captured by the thinner PAN fibers, while the oily particles can hardly be seen on the thicker PS fibers, which also proves that the PS microfibers served as a support improve the air permeability of the filter and the PAN nanofibers are responsible for intercepting particles. As a PBS fiber membrane with self-powered structure constructed together with PAN/PS composite mat, its filtration performance was also measured (Fig. 5c). The $PM_{0.3}$ filtration efficiency and the pressure drop of PBS fiber membrane are 86.5%, and 36 Pa. Even after 20 min of filtration, its filtration efficiency remains to be 77%, while the pressure drop is 55 Pa. Compared to pure PBS fiber membrane and PAN/PS fiber composite mat, the PAN/PS-PBS fiber mat exhibited enhanced filtration efficiency (Fig. 5d). The $PM_{0.3}$ filtration efficiency of filter reached to 98.6%. After 40 min of filtration, the filtration efficiency decreased slightly, but remains to be above 94%. Take out the membrane and charge it by contact in the way shown in Fig. 4d, and then measure the filtration efficiency again. It was found that the filtration efficiency has been significantly improved, and the filtration efficiency of $PM_{0.3}$ has risen to 98.3%, which indicates that the electrostatic capture of surface charge plays an important role in the filtration of particulate matter. After filtering for 5 min, the filtering performance drops to the level before charging. Within 50 min after that, the charging experiment was conducted to measure filtration efficiency for five times circularly, and the surface potentials of the two membranes were also obtained. It can be found that

the filtration efficiency was improved significantly after charging, and the surface potential of PAN/PS fiber mats and PBS fiber mats also recovered to about -3.5 kV and about 2 kV. Overall, it shows that the surface potential of the fiber membrane can be recovered through the contact- separation of the fiber membrane, thus restoring the filtration performance of the fiber membrane. The quality factor and air pressure drop of the self-powered filter were 0.076 and 53 Pa (Fig. 5e), respectively, which is much higher than the PAN/PS fiber composite mat and PBS fiber membrane. With the increase of filtration time, filtration efficiency and quality factor gradually decrease. Interestingly, once the filter material is frictionally recharged, the filtration efficiency and the quality factor will be also improved. However, due to the increase in pressure drop, the quality factor will not return to the original 0.076. On the one hand, coarse PS fibers provide a good airflow path as a support, while fine PAN fibers can effectively physically intercept particles. On the other hand, through contact charging, the surface of the fiber membrane carries a large amount of surface charge, and electrostatic force is used to improve the capture of particles. This process does not affect the permeability of the material. This allows the material to maintain excellent filtration efficiency at a low pressure drop. The self-powered structure driven by breathing ensures the continuous existence of surface charges on the material, so that the filtration efficiency can remain stable for a long time. In addition, due to the presence of PS fibers, the porous structure inside the material is fluffy, which improves the dust holding rate of the fiber material, and is also the reason why the performance of the filter material can be stable for a long time.

Fig. 5f, g shows the filtration efficiency, pressure drop and QF of the commercial mask middle layer (PP melt blown nonwoven) and the prepared self-powered filter under the same filtration conditions. The TENG filter structure in this work has more excellent filtration efficiency under extremely harsh air conditions. The filtration efficiency for $PM_{0.3}$ is more than 98%, much higher than that of PP melt blown nonwoven ($\eta_{PM_{0.3}}=80\%$). The pressure drop is only 10 Pa higher than that of PP melt blown nonwoven. And because the breath drives its constant contact charging, the filtering efficiency can remain stable for a long time. As shown in Fig. 5g, the quality factor of the PAN/PS-PBS self-powered filter device is higher than that of PP melt blown nonwoven, with a QF value of 0.076, while the QF of PP melt blown nonwoven is only 0.045. Due to the initial mass concentration of $PM_{2.5}$ in this work filtration test is approximately $23,000 \mu\text{g}/\text{m}^3$, excessive particle mass concentration leads to a thick layer of dust cake on the surface of the material after continuous filtration for about 2 h, which affects the experimental results. Placing the PP melt blown cloth commonly used for the middle layer of masks under the same experimental conditions, the filtration performance decreased to 40% after 60 min (**Fig. 5f**), indicating that the device cannot measure the long-term filtration performance of filter media. Therefore, the experiment only shows the filtering results of 100 min. To test the durability of the performance of the filter material, **Fig. S7** shows the filtration efficiency measured within 48 h at a gas flow rate of 32 L/min (close to human respiration [18]) when the material is placed in an experimental environment (severely polluted) at 30 °C, 50% RH, and a mass concentration of $PM_{2.5}$ of $214.3 \pm 1.6 \mu\text{g}/\text{m}^3$. Obviously, the filtration

efficiency of the filter material to $PM_{0.3}$ can still reach 99.43% after 48 h. It indicates that the effective time of the filter material meets the requirements of the mask (8 h). In addition, the tensile properties of PP melt blown fabric, PAN/PS composite mat and PBS fiber mat under the same conditions were also measured through the multifunctional fabric tester. As shown in Fig. 5h, the tensile performance of PBS fiber membrane was similar to that of PP melt blown nonwoven, while the breaking strength of PAN/PS composite mat was relatively low, but it has a higher breaking elongation. The surface potential of the self-powered filter after 25, 50, 75, and 100 consecutive contact separations was shown in Fig. S8. Even after 100 charging experiments, the fiber membrane surface still has a significant surface potential, and the fiber membrane is not damaged or broken, which proves that the self-powered filter has good long-term cycle performance. In addition, an attempt can be made to prepare a fiber membrane that can be charged in contact with the skin by introducing a material that can generate inductive charges in contact with the skin. This will greatly simplify the self-powered structure, and contact with soft skin will reduce the wear of the fiber membrane and improve the reusability of the material. This experimental assumption will be explored in the next step of research. The above results shows that the PAN/PS-PBS self-powered filter device meets the requirements of respirator both in terms of filtering efficiency and mechanical properties, and achieves the expected assumption of the experiment.

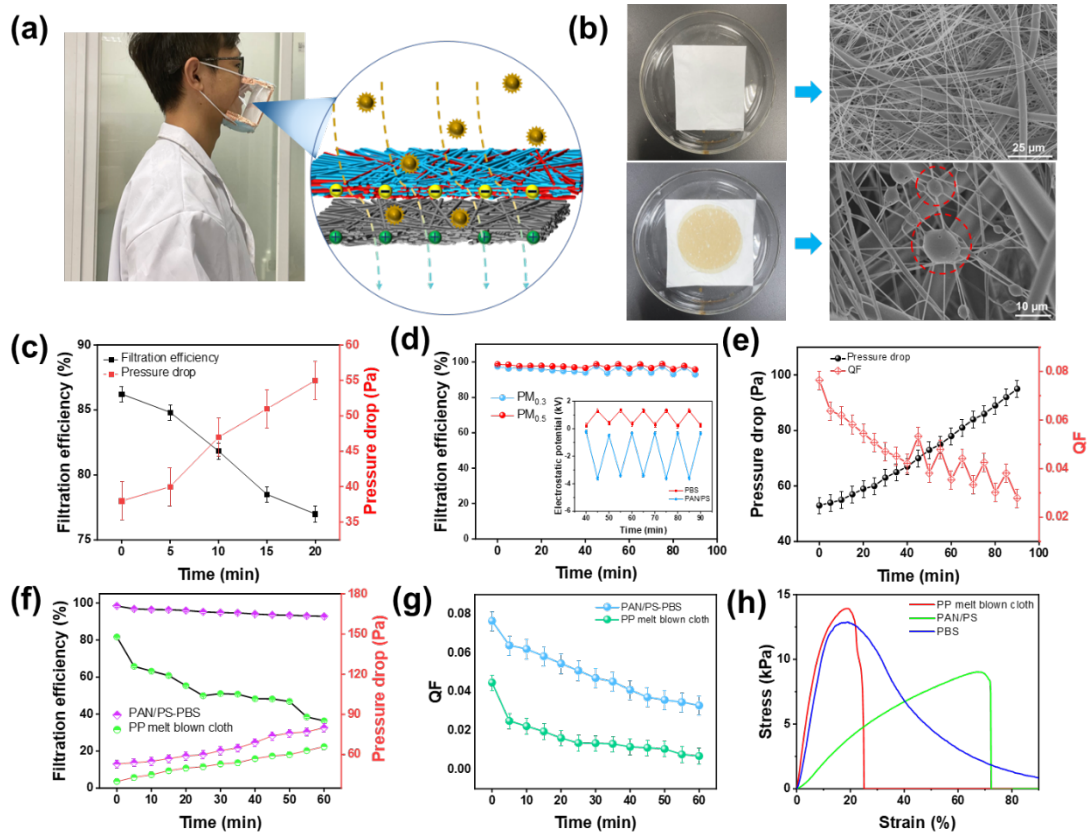


Fig. 5 (a) Physical diagram of arch self-powered filter structure, (b) Physical diagram before and after PAN/PS composite mat filtration and SEM diagram, (c) Filtering efficiency and pressure drop of PBS fiber membrane for $PM_{0.3}$, (d) Filtering efficiency of arch structure for $PM_{0.3}$ within 90 min and recovery of filtering efficiency when cycling charging after 40 min, (e) Pressure drop and QF of arch structure during filtration, (f) Comparison of filtration efficiency and pressure drop of $PM_{0.3}$ of arch structure and commercial mask middle layer (PP melt blown fabric), (g) QF of arch structure and PP melt blown fabric, (h) Comparison of tensile properties of arch structure and PP melt blown fabric.

4. Conclusion

In this work, a composite mat composed of coarse PS microfibers and PAN

nanofibers was demonstrated, in which PS fibers served as the support frame provided good air permeability, while the fine PAN fibers provided good filtration efficiency, achieving a good balance between filtration performance and permeability. By comparing and analyzing the difference of filtration efficiency, pressure drop of various PAN/PS fiber composite mats and the electric field intensity of single fibers within the mat, it was found that when the PAN/PS1-1 fiber membrane exhibited optimal filtration property. At an air flow rate of 32 L/min and 85 L/min, the $PM_{0.3}$ filtration efficiency of the fiber membrane reached 99.98% and 97.53%, respectively, while the pressure drop was only 35 Pa and 85 Pa. Even in severe air environment ($\rho_{PM_{2.5}}: 23,000 \mu\text{g}/\text{m}^3$), the $PM_{0.3}$ filtration efficiency of the fiber membrane can still reach to 94%. In addition, the PBS fiber membrane with low electronegativity was combined with the PAN/PS composite mat and anti-adhesion paper to create a TENG-based filter. Through the contact-separation of the fiber membrane, the electrons move in a directional route, which enables the surface of the fiber membrane of the induced charges. The two fiber membranes have an open-circuit voltage of 8 V during the contact-separation process. And the surface potential of the PAN/PS composite mat and PBS fiber membrane reached to -3.5 ± 0.2 kV and 2 ± 0.2 kV respectively. The self-powered fiber mat still has a significant surface potential after 100 charging experiments, and the fiber membrane has not been damaged or broken, indicating good long-term cycling performance of the self- powered filter. The TENG mat was assembled with a wearable frame to form an air filter mask, which can achieve higher air filtration efficiency ($\eta_{PM_{0.3}}=98.6\%$) at a low pressure drop (53 Pa). This work achieves long-term and

efficient filtration of particulate matter through friction charging, and has broad application prospects in the field of air filtration.

Conflicts of interest:

The authors declare no competing financial interest.

Acknowledgments

The authors thank the financial support from the National Key Research and Development Program of China (2022YFB3804905, 2022YFB3804900, and 2019YFE0111200), National Natural Science Foundation of China (51972063, 22075046), Natural Science Foundation of Fujian Province (2022J01568 and 2020J06038), State Key Laboratory for Modification of Chemical Fibers and Polymer Materials (KF2320), State Key Laboratory of New Textile Materials and Advanced Processing Technologies (FZ2021012).

References

- [1] Wang S, Li JN, Cao YH, Gu JW, Wang YF, Chen SG. Non-leaching, rapid bactericidal and biocompatible polyester fabrics finished with benzophenone terminated N-halamine. *Adv Fiber Mater.* **2022**, 4: 119.
- [2] Liu H, Huang JY, Mao JJ, Chen Z, Chen GQ, Lai YK. Transparent antibacterial nanofiber air filters with highly efficient moisture resistance for sustainable particulate matter capture. *iScience.* **2019**, 19: 214.
- [3] Sun YJ, Zhang X, Zhang M, Ge MZ, Wang JC, Tang YX, Zhang YY, Mi J, Cai WL,

- Lai YK, Feng Y. Rational design of electrospun nanofibers for gas purification: Principles, opportunities, and challenges. *Chem Eng J.* **2022**, 446: 137099.
- [4] Liu J, Tian EZ, Zhang SL, Kong DY, Liu KH, Bai XD, Liu KH. The rise of two-dimensional-material-based filters for airborne particulate matter removal. *Adv Fiber Mater.* **2022**, 162: 42765.
- [5] Gou YK, Hao YY, Cai WL, Huang JY, Lai YK. Rational designed ZIF-8@PDA@PDMS composite sponge for efficient and sustainable particulate matter filtering under harsh environment. *Particuology.* **2023**, 76: 141.
- [6] Wang G, Wang L, Meng ZY, Su XL, Jia C, Qiao XL, Pan SW, Chen YJ, Cheng YH, Zhu MF. Visual detection of COVID-19 from materials aspect. *Adv Fiber Mater.* **2022**, 4: 1304.
- [7] Luo JJ, Liu H, Hua SC, Song L. The correlation of PM_{2.5} exposure with acute attack and steroid sensitivity in asthma. *Biomed Res Int.* **2022**, 2022: 2756147.
- [8] Liu GX, Nie JH, Han CB, Jiang T, Yang ZW, Pang YK, Xu L, Guo T, Bu TZ, Zhang C, Wang ZL. Self-powered electrostatic adsorption face mask based on a triboelectric nanogenerator. *ACS Appl Mater Interfaces.* **2018**, 10: 7126.
- [9] Bai Y, Han CB, He C, Gu GQ, Nie JH, Shao JJ, Xiao TX, Deng CR, Wang ZL. Washable multilayer triboelectric air filter for efficient particulate matter PM_{2.5} removal. *Adv Funct Mater.* **2018**, 28: 1706680.
- [10] Zhu CY, Maharajan K, Liu KC, Zhang Y. Role of atmospheric particulate matter exposure in COVID-19 and other health risks in human: A review. *Environ Res.* **2021**, 198: 111281.

- [11] Mao JJ, Tang YX, Wang YD, Huang JY, Dong XL, Chen Z, Lai YK. Particulate matter capturing via naturally dried ZIF-8/graphene aerogels under harsh conditions. *iScience*. **2019**, 16: 133.
- [12] Landkocz Y, Ledoux F, Andre V, Cazier F, Genevray P, Dewaele D, Martin PJ, Lepers C, Verdin A, Courcot L, Boushina S, Sichel F, Gualtieri M, Shirali P, Courcot D, Billet S. Fine and ultrafine atmospheric particulate matter at a multi-influenced urban site: Physicochemical characterization, mutagenicity and cytotoxicity. *Environ Pollut*. **2017**, 221: 130.
- [13] Lin SZ, Wang SX, Yang W, Chen SW, Xu ZS, Mo XW, Zhou H, Duan JJ, Hu B, Huang L. Trap-induced dense monocharged perfluorinated electret nanofibers for recyclable multifunctional healthcare mask. *ACS Nano*. **2021**, 15: 5486.
- [14] Wang HT, Xu H, Li H, Liu X, Du ZQ, Yu WD. Electrospun polyurethane/zeolitic imidazolate framework nanofibrous membrane with superior stability for filtering performance. *ACS Appl Polym Materfaces*. **2021**, 3: 710.
- [15] Xiong SW, Fu PG, Zou Q, Chen LY, Jiang MY, Zhang P, Wang ZG, Cui LS, Guo H, Gai JG. Heat conduction and antibacterial hexagonal boron nitride/polypropylene nanocomposite fibrous membranes for face masks with long-time wearing performance. *ACS Appl Mater Interfaces*. **2021**, 13: 196.
- [16] Liao L, Xiao W, Zhao MV, Yu XZ, Wang HT, Wang QQ, Chu S, Cui Y. Can N95 respirators be reused after disinfection? How many times? *ACS Nano*. **2020**, 14: 6348.
- [17] Zhu J, Jiang Q, He X, Li X, Wang L, Zheng L, Jing P, Chen M. Filtration efficiency of N95 filtering facepiece respirators during multi-cycles of '8-hour simulated

- donning plus disinfection'. *J Hosp Infect.* **2022**, 127: 91.
- [18] Zhao M, Liao L, Xiao W, Yu XZ, Wang HT, Wang QQ, Lin YL, Kilinc-Balci FS, Price A, Chu L, Chu MC, Chu S, Cui Y. Household materials selection for homemade cloth face coverings and their filtration efficiency enhancement with triboelectric charging. *Nano Lett.* **2020**, 20: 5544.
- [19] Wang QF, Wei YZ, Li WB, Luo XZ, Zhang XY, Di JC, Wang GQ, Yu JH. Polarity-dominated stable N97 respirators for airborne virus capture based on nanofibrous membranes. *Angew Chem Int Edit.* **2021**, 60: 23756.
- [20] Faridi-Majidi R, Norouz F, Boroumand S, Tabatabaei SN, Faridi-Majidi R. Decontamination assessment of nanofiber-based N95 masks. *Environ Sci Pollut R.* **2022**, 29: 80411.
- [21] Rule A, Ramachandran G, Koehler K. Comment on aerosol filtration efficiency of common fabrics used in respiratory cloth masks: questioning their findings. *ACS Nano.* **2020**, 14: 10756.
- [22] Huber T, Goldman O, Epstein AE, Stella G, Sakmar TP. Principles and practice for SARS-CoV-2 decontamination of N95 masks with UV-C. *Biophys J.* **2021**, 120: 2927.
- [23] Santra PK, Singh AK, Kulkarni GU, Kundu S, Rao TIS, Ganesha MK. Aesthetically acceptable, breath friendly triboelectric face masks: design, fabrication, and its efficacy. *Energy Technol-Ger.* **2021**, 9: 12.
- [24] Lubrano R, Bloise S, Marcellino A, Ciolli CP, Testa A, De Luca E, Dilillo A, Mallardo S, Isoldi S, Martucci V, Sanseviero MT, Del Giudice E, Malvaso C, Iacovelli C, Leone R, Iorfida D, Ventriglia F. Effects of N95 mask use on pulmonary

- function in children. *J Pediatr-Us*. **2021**, 237: 143.
- [25] Fan FR, Tian ZQ, Wang ZL. Flexible triboelectric generator! *Nano Energy*. **2012**, 1: 328.
- [26] Zhang C, Tang W, Han CB, Fan FR, Wang ZL. Theoretical comparison, equivalent transformation, and conjunction operations of electromagnetic induction generator and triboelectric nanogenerator for harvesting mechanical energy. *Adv Mater*. **2014**, 26: 3580.
- [27] Ghatak B, Banerjee S, Ali SKB, Bandyopadhyay R, Das N, Mandal D, Tudu B. Design of a self-powered triboelectric face mask. *Nano Energy*. **2021**, 79: 105387.
- [28] Hao RF, Yang S, Yang K, Zhang ZY, Wang T, Sang SB, Zhang HL. Self-powered air filter based on an electrospun respiratory triboelectric nanogenerator. *ACS Appl Energ Mater*. **2021**, 4: 14700.
- [29] Lu T, Cui JX, Qu QL, Wang YL, Zhang J, Xiong RH, Ma WJ, Huang CB. Multistructured electrospun nanofibers for air filtration: a review. *ACS Appl Mater Interfaces*. **2021**, 13: 23293.
- [30] Jiang SH, Schmalz H, Agarwal S, Greiner A. Electrospinning of ABS nanofibers and their high filtration performance. *Adv Fiber Mater*. **2020**, 2: 34.
- [31] Zong DD, Zhang XX, Yin X, Wang F, Yu JY, Zhang SC, Ding B. Electrospun fibrous sponges: principle, fabrication, and applications. *Adv Fiber Mater*. **2022**, 4: 1434.
- [32] Deng YK, Lu T, Cui JX, Samal SK, Xiong RH, Huang CB. Bio-based electrospun nanofiber as building blocks for a novel eco-friendly air filtration membrane: A

- review. *Sep Purif Technol.* **2021**, 277: 119623.
- [33] Cui JX, Li FH, Wang YL, Zhang QL, Ma WJ, Huang CB. Electrospun nanofiber membranes for wastewater treatment applications. *Sep Purif Technol.* **2020**, 250: 117116.
- [34] Gu GQ, Han CB, Lu CX, He C, Jiang T, Gao ZL, Li CJ, Wang ZL. Triboelectric nanogenerator enhanced nanofiber air filters for efficient particulate matter removal. *ACS Nano.* **2017**, 11: 6211.
- [35] Zhang RC, Xu Q, Bai S, Hai J, Cheng L, Xu GQ, Qin Y. Enhancing the filtration efficiency and wearing time of disposable surgical masks using TENG technology. *Nano Energy.* **2021**, 79: 105434.
- [36] Cho YJ, Son Y, Ahn J, Lim H, Ahn S, Lee JY, Bae PK, Kim I. Multifunctional filter membranes based on self-assembled core-shell biodegradable nanofibers for persistent electrostatic filtration through the triboelectric effect. *ACS Nano.* **2022**, 14: 19451.
- [37] Fu Q, Liu YH, Liu T, Mo JL, Zhang WL, Zhang S, Luo B, Wang JL, Qin Y, Wang SF, Nie SX. Air-permeable cellulosic triboelectric materials for self-powered healthcare products. *Nano Energy.* **2022**, 102: 107739.
- [38] Li X, Wang C, Huang XH, Zhang TH, Wang XF, Min MH, Wang LM, Huang HL, Hsiao BS. Anionic surfactant-triggered steiner geometrical poly (vinylidene fluoride) nanofiber/nanonet air filter for efficient particulate matter removal. *ACS Appl Mater Inter.* **2018**, 10: 42891.
- [39] Liu H, Zhang SC, Liu LF, Yu JY, Ding B. High-performance PM_{0.3} air filters using

- self-polarized electret nanofiber/nets. *Adv Funct Mater.* **2020**, 30: 13.
- [40] Zhu CY, Yang F, Xue TT, Wali Q, Fan W, Liu TX. Metal-organic framework decorated polyimide nanofiber aerogels for efficient high-temperature particulate matter removal. *Sep Purif Technol.* **2022**, 300: 121881.
- [41] Fan M, Zhang B, Fan L, Chen F, Fu Q. Adsorbability of modified PBS nanofiber membrane to heavy metal ions and dyes. *J Polym Environ.* **2021**, 29: 3029.
- [42] Shao ZG, Jiang JX, Wang X, Li WW, Fang L, Zheng GF. Self-powered electrospun composite nanofiber membrane for highly efficient air filtration. *Nanomaterials.* **2020**, 10: 1706.
- [43] Sathirapongsasuti N, Panaksri A, Boonyagul S, Chutipongtanate S, Tanadchangsang N. Electrospun fibers of polybutylene succinate/graphene oxide composite for syringe-push protein absorption membrane. *Polymers.* **2021**, 13: 2042.
- [44] Khalid B, Bai XP, Wei HH, Huang Y, Wu H, Cui Y. Direct blow-spinning of nanofibers on a window screen for highly efficient PM_{2.5} removal. *Nano Lett.* **2017**, 17: 1140.
- [45] Cai RR, Li SZ, Zhang LZ, Lei Y. Fabrication and performance of a stable micro/nano composite electret filter for effective PM_{2.5} capture. *Sci Total Environ.* **2020**, 725: 138297.
- [46] Lu N, Yan LJ, Ma YJ, Sun HX, Zhu ZQ, Liang WD, Li JY, Li A. Electrospun modified SiO₂ nanofiber membranes as superamphiphobic self-cleaning filters with high heat stability for efficient particle matter capture. *Acs Appl Nano Mater.* **2022**, 5: 9871.

- [47] Li YY, Cao LT, Yin X, Si Y, Yu JY, Ding B. Ultrafine, self-crimp, and electret nanowool for low-resistance and high-efficiency protective filter media against PM_{0.3}. *J Colloid Interface Sci.* **2020**, 578: 565.
- [48] Liu C, Hsu PC, Lee HW, Ye M, Zheng GY, Liu NA, Li WY, Cui Y. Transparent air filter for high-efficiency PM_{2.5} capture. *Nat Commun.* **2015**, 6: 6205.
- [49] Lee J, Kim J. Material properties influencing the charge decay of electret filters and their impact on filtration performance. *Polymers.* **2020**, 12: 721.